

Clustering of luminous red galaxies II: small scale redshift space distortions

Anna Cabré, Enrique Gaztañaga

Institut de Ciències de l'Espai, CSIC/IEEC, Campus UAB, F. de Ciències, Torre C5 par-2, Barcelona 08193, Spain

7 November 2018

ABSTRACT

This is the second paper of a series where we study the clustering of LRG galaxies in the latest spectroscopic SDSS data release, DR6, which has 75000 LRG galaxies covering over $1 \text{ Gpc}^3/h^3$ for $0.15 < z < 0.47$. Here we focus on modeling redshift space distortions in $\xi(\sigma, \pi)$, the 2-point correlation in separate line-of-sight and perpendicular directions, at small scales and in the line-of-sight. We show that a simple Kaiser model for the anisotropic 2-point correlation function in redshift space, convolved with a distribution of random peculiar velocities with an exponential form, can describe well the correlation of LRG at all scales. We show that to describe with accuracy the so called "fingers-of-God" (FOG) elongations in the radial direction, it is necessary to model the scale dependence of both bias b and the pairwise rms peculiar velocity σ_{12} with the distance. We show how both quantities can be inferred from the $\xi(\sigma, \pi)$ data. From $r \simeq 10 \text{ Mpc}/h$ to $r \simeq 1 \text{ Mpc}/h$, both the bias and σ_{12} are shown to increase by a factor of two: from $b = 2$ to $b = 4$ and from $\sigma_{12} = 400$ to $800 \text{ Km}/s$. The later is in good agreement, within a 5 percent accuracy in the recovered velocities, with direct velocity measurements in dark matter simulations with $\Omega_m = 0.25$ and $\sigma_8 = 0.85$.

1 INTRODUCTION

The luminous red galaxies (LRGs) are selected by color and magnitude to obtain intrinsically red galaxies in Sloan Digital Sky Survey (SDSS) (Eisenstein et al 2001). These galaxies trace a big volume, around $1 \text{ Gpc}^3 h^{-3}$, which make them perfect to study large scale clustering or smaller scales with larger statistics. In this paper we focus on the 2-point correlation function $\xi(\sigma, \pi)$ on the smaller scales, where the non-linear bias and the random peculiar velocities can complicate the analysis. Our motivation is to provide a model that can explain the observed $\xi(\sigma, \pi)$ of the LRG galaxies. Such a model does not exist right now and we are not aware of any attempt to reproduce the $\xi(\sigma, \pi)$ in the detail we will explore here. LRG galaxies seem to display larger "Fingers-of-God" (Jackson 1972) than regular galaxies, is this evidence for larger velocities? If so, is this evidence that LRG trace stronger gravitational potentials? We will show that a simple Kaiser model for the anisotropic 2-point correlation function in redshift space, convolved with a distribution of random peculiar velocities with an exponential form, can describe well the correlation of LRG at all the scales. To describe with accuracy the so called "fingers-of-God" (FOG) elongations in the radial direction, it is necessary to model

the scale dependence of both bias b and the pairwise rms peculiar velocity σ_{12} with the distance.

In Paper I (Cabré and Gaztañaga 2008) of this series, we have analyzed larger scales and present the basis for this work, including more detailed theory, error and systematic effects.

On large scales, the density fluctuations are small enough to be linearized, and can be used to constrain cosmological parameters, since we can assume that the clustering is well described by (linearly biased) dark matter (see Paper I). On smaller scales, we can learn about the relation of galaxies to dark matter through the biased clustering of halos. This range of distances can be fitted by a power law, but there are small deviations that can be understood in the theory of the halo occupation distribution. The transition between galaxy pairs of the same halo and galaxy pairs that belong to different halo, occurs around $1 \text{ Mpc}/h$. When moving to scales smaller than $1 \text{ Mpc}/h$, in the 1-halo term, we can see processes more complex that modify the galaxy clustering, such as dynamical friction, tidal interactions, stellar feedback, and other dissipative processes.

We use the most recent spectroscopic SDSS data release, DR6 (Adelman-McCarthy et al 2006), to perform the study of small scales in the anisotropic 2-point correla-

tion function, and its derivatives projected correlation function and real-space correlation function. LRGs are supposed to be red old elliptical galaxies, which are usually passive galaxies, with relatively low star formation rate. They have steeper slopes in the correlation function than the rest of galaxies, since they are supposed to reside in the centers of big halos, inducing non-linear bias dependent on scale, for small scales.

The same LRGs (but with reduced area) have been studied from different points of view. Zehavi et al (2005) study LRGs at intermediate scales (0.3 to 40Mpc/h), where they calculate the projected correlation function, the monopole and real-space correlation function to study mainly linear bias, non-linear bias and the differences between luminosities. They find that there are differences from a power law for scales smaller than 1Mpc/h and they find no strong evolution for LRG. At smaller scales, Eisenstein et al (2005) did a cross-correlation between spectroscopic LRG with photometric main sample in order to reduce shot-noise in small scales clustering. They conclude that the clustering is higher for most luminous galaxies. Moreover, LRG have a scale dependent bias on luminosity, while for normal galaxies the luminosity bias is scale independent. LRG galaxies are surrounded by other red galaxies near them, which seem to be approaching the center LRG galaxy. Finally, Masjedi et al (2006) deal with very small scale clustering to scales smaller than 55" by cross-correlating the spectroscopic LRG sample and the targeted imaging sample and find that the correlation function from 0.01-8Mpc/h is really close to a power law with slope -2, but there are still some features that diverge from the power law.

The small scale slope depends on the interplay between two factors which control how the correlation function of galaxies is related to that of the underlying matter : the number of galaxies within a dark matter halo (HOD) and the range of halo masses which contain more than one galaxy (Benson et al 2000). LRGs are to be found in halos with the median of the distribution occurring at $3 \cdot 10^{13} M_{\odot}/h$, estimated using weak lensing measurements (Mandelbaum et al 2006). Almeida et al (2008) find with simulations that 25% of LRGs at $z = 0.24$ are satellite galaxies, which play an important role in the form of the small scale correlation function, as well as the pairwise velocity dispersion, and also provide information about galaxy formation and evolution. Zheng et al (2008), who study HOD in LRG clustering, find that the satellite fraction is small (5-5% for $M_g < -21.2$) and decreases with LRG luminosity.

Slosar et al (2006) show that pairwise velocity distribution in real space is a complicated mixture of host-satellite, satellite-satellite and two-halo pairs. The peak value is reached at around 1Mpc/h and does not reflect the velocity dispersion σ_{12} of a typical halo hosting these galaxies, but is instead dominated by the sat-sat pairs in high-mass clusters. Different groups have found this dependence of σ_{12} on the

scale (Zehavi et al 2002, Hawkins et al 2003, Jing and Borner 2004, Li et al 2006, Van den Bosch 2007, Li et al 2007). They also find that σ_{12} depends on luminosity, with higher values for both large and small luminosities, but this tendency can not be predicted by the halo model. Li et al (2006, 2007) add that redder galaxies have stronger clustering and larger velocities at all scales, so they move in strongest gravitational fields. Tinker et al (2007) use the halo occupation distribution framework to make robust predictions of the pairwise velocity dispersion (PVD). They assume that central galaxies move with the center of mass of the host halo and satellite galaxies move as dark matter. The pairs that involve central galaxies have a lower dispersion, so the fraction of satellites strongly influences both the luminosity and scale dependence of the PVD in their predictions. At r between 1 and 2 Mpc/h, the PVD rapidly increases with smaller separation as satellite-satellite one-halo pairs from massive halos dominate. At $r < 1$ Mpc/h, the PVD decreases towards smaller scales because central-satellite one-halo pairs become more common. At $r > 3$ Mpc/h, the PVD is dominated by two-halo central galaxy pairs, and reach a constant value.

LRGs have also been analyzed at higher redshifts ($z=0.55$) with the 2dF-SDSS LRG and QSO Survey (2SLAQ, Cannon et al 2007). Ross et al (2007), Da Ângela et al (2008) and Wake et al (2008) analyze the redshift distortions in the LRGs and quasars for this catalog. For part of our analysis we have followed the method explained in Hawkins et al (2003), an extensive analysis of the redshift distortions in the 2dF catalog.

Here we define the parameters that we assume during all this work, which are motivated by recent results of WMAP, SNIa and previous LSS analysis: $n_s = 0.98$, $\Omega_b = 0.045$, $h = 0.72$ and flat geometry. Unless otherwise said, we use $\Omega_m = 0.25$ and $\sigma_8 = 0.85$, both obtained from paper I. We will use the power spectrum analytical form for dark matter by Eisenstein and Hu (1998), and the non-linear fit to halo theory by Smith et al (2003).

2 MODELING REDSHIFT-SPACE

We follow the modeling given in more detailed in Paper I (Cabré and Gaztañaga 2008). Here we just show the main equations related to this work. In the large-scale linear regime and in the plane-parallel approximation (where galaxies are taken to be sufficiently far away from the observer that the displacements induced by peculiar velocities are effectively parallel), the distortion caused by coherent infall velocities takes a particularly simple form in Fourier space (Kaiser 1987):

$$P_s(k) = (1 + \beta\mu_k^2)^2 P(k). \quad (1)$$

where $P(k)$ is the power spectrum of density fluctuations δ , μ is the cosine of the angle between k and the line-of-sight, the subscript s indicates redshift space, and β is the growth rate of growing modes in linear theory.

The observed value of β is

$$\beta = \frac{f(\Omega_m)}{b} \equiv \frac{1}{b} \frac{d \ln D}{d \ln a} \quad (2)$$

where b is the bias between galaxies and dark matter, $f(\Omega_m)$ and $D(\Omega_m)$ are the linear growth density and velocity factors. Here we use Hamilton (1992) who translated Kaiser results into real space $\xi'(\sigma, \pi)$ (see Eq.(8) in Paper I). We then convolve it with the distribution function of random pairwise velocities, $f(v)$, to give the final model $\xi(\sigma, \pi)$ (Peebles 1980):

$$\xi(\sigma, \pi) = \int_{-\infty}^{\infty} \xi'(\sigma, \pi - v/H(z)/a(z)) f(v) dv \quad (3)$$

We represent the random motions by an exponential form (Szalay et al, 1998),

$$f(v) = \frac{1}{\sigma_{12}\sqrt{2}} \exp\left(-\frac{\sqrt{2}|v|}{\sigma_{12}}\right) \quad (4)$$

where σ_{12} is the pairwise peculiar velocity dispersion.

It is well known that σ_{12} depends on the real separation between particles $r = \sqrt{\sigma^2 + \pi_{real}^2}$, where $\pi_{real} = \pi - v/H(z)/a(z)$. The pairwise velocity dispersion is roughly constant for $r > 5Mpc/h$, but increases towards smaller values of r . To use Eq.(3) and Eq.(4) with σ_{12} depending on r , we do the following. For each value of the velocity v in the integral, we estimate the real distance $r = \sqrt{\sigma^2 + \pi_{real}^2}$ and the value of $\sigma_{12} = \sigma_{12}(r)$ that enters in $f(v)$. We have checked that for $\sigma > 2Mpc/h$, this exact method is very similar to assuming that σ_{12} is fixed for each σ and it is constant along the line-of-sight π , so we can change σ_{12} depending on σ , rather than r . This has some practical advantages over the exact method.

We define the multipoles of $\xi(\sigma, \pi)$ as

$$\xi_\ell(s) = \frac{2\ell+1}{2} \int_{-1}^{+1} \xi(\sigma, \pi) P_\ell(\mu) d\mu. \quad (5)$$

where μ is cosine of the angle to the line-of-sight π . The monopole $\xi(s) \equiv \xi_0(s)$ is also called the redshift space correlation function. The real-space correlation function can be estimated from the projected correlation function, $\Xi(\sigma)$, by integrating the redshift distorted $\xi(\sigma, \pi)$ along the line-of-sight π :

$$\Xi(\sigma) = 2 \int_0^\infty \xi(\sigma, \pi) d\pi \quad (6)$$

Davis and Peebles (1983) show that $\Xi(\sigma)$ is directly related to the real-space correlation function.

$$\Xi(\sigma) = 2 \int_\sigma^\infty \frac{r\xi(r)dr}{(r^2 - \sigma^2)^{\frac{1}{2}}}. \quad (7)$$

It is possible to estimate $\xi(r)$ by directly inverting $\Xi(\sigma)$ (Saunders et al 1992). We can write Eq.(7) as,

$$\xi(r) = -\frac{1}{\pi} \int_r^\infty \frac{(d\Xi(\sigma)/d\sigma)}{(\sigma^2 - r^2)^{\frac{1}{2}}} d\sigma. \quad (8)$$

Assuming a step function for $\Xi(\sigma) = \Xi_i$ in bins centered on σ_i , and interpolating between values,

$$\xi(\sigma_i) = -\frac{1}{\pi} \sum_{j \geq i} \frac{\Xi_{j+1} - \Xi_j}{\sigma_{j+1} - \sigma_j} \ln \left(\frac{\sigma_{j+1} + \sqrt{\sigma_{j+1}^2 - \sigma_i^2}}{\sigma_j + \sqrt{\sigma_j^2 - \sigma_i^2}} \right) \quad (9)$$

for $r = \sigma_i$.

Once we recover the real-space correlation function, we can also estimate the ratio of the redshift-space correlation function, $\xi(s)$, to the real-space correlation function, $\xi(r)$, which gives an estimate of the redshift distortion parameter, β , on large scales:

$$\frac{\xi(s)}{\xi(r)} = 1 + \frac{2\beta}{3} + \frac{\beta^2}{5}. \quad (10)$$

3 STUDY OF THE ERRORS

A detailed account of errors is given in Paper I. Basically we use mock catalogs to estimate what we call the Monte Carlo (MC) errors. Mock catalogs are build out of very large numerical simulations run in the super computer Mare Nostrum in Barcelona by MICE consortium (www.ice.cat/mice). The simulation contains 2048^3 dark matter particles, in a cube of side $7680Mpc/h$, $\Omega_M = 0.25$, $\Omega_b = 0.044$, $\sigma_8 = 0.8$, $n_s = 0.95$ and $h = 0.7$. We use both dark matter and groups. There is no bias in the dark matter mocks, so $\beta = \frac{\Omega_m(z)^{0.55}}{b} = 0.62$ (where $\Omega_m(z) = \Omega_m(1+z)^3/(\Omega_m(1+z)^3 + 1 - \Omega_m)$ and $b = 1$). In this paper, we use group mocks with $M > 2.2 \times 10^{13} M_\odot$ ($b = 1.9$, $\beta = 0.25$) at $z = 0$, which are similar to real LRG galaxies in its clustering properties.

For the jackknife (JK) error, we obtain the different realizations directly from the data, dividing the catalog in M zones, and we consider that each realization is all the catalog except from one of these JK zones. In this case, as the realizations are clearly not independent, we multiply the covariance matrix by a factor $(M - 1)$ to account for this effect (see Paper I for more details).

To analyze data we prefer to use a model independent error, such as the JK error above. The MC error based on simulations depends on the model that we have used and in particular in the overall normalization, which is similar to LRG for group simulations but can have slight differences. We use the MC errors to probe the accuracy of JK errors in the same simulations.

In Paper I (Cabr e and Gazta naga 2008), we present the errors in the redshift space correlation function $\xi(\sigma, \pi)$ (bin=5Mpc/h), the monopole $\xi(s)$ and the quadrupole $Q(s)$. Here we study the errors in the $\xi(\sigma, \pi)$ (bin=1Mpc/h and 0.2Mpc/h), perpendicular projected function $\Xi(\sigma)$ and in

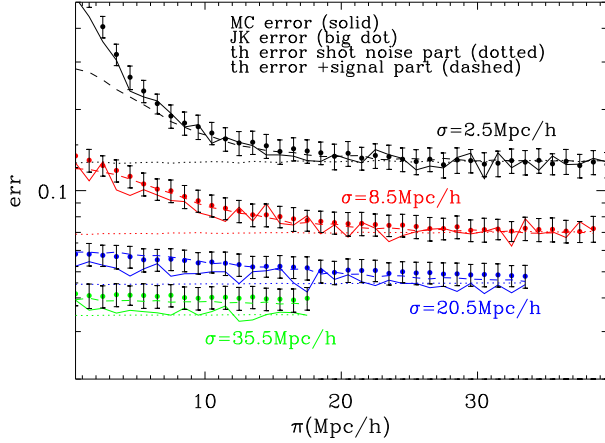


Figure 2. We compare different error estimators for $\xi(\sigma, \pi)$ with 1Mpc/h of bin for MICE group mocks with $b = 1.9$. We fix the perpendicular distance σ and move along the line-of-sight π as indicated in the figure. The errors are: MC (solid line), theory with (dashed) and without (dotted) the signal part of the error, and JK (big dots with errorbars). As we move to higher σ (lower amplitudes), JK starts to fail, but the analytical and MC errors there agree well.

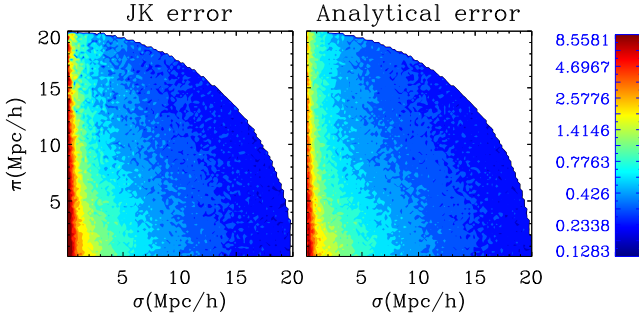


Figure 3. We compare different error estimators for $\xi(\sigma, \pi)$ with 0.2Mpc/h of binning for LRG real data: JK and analytical. As in the case of bin=1Mpc/h, JK seems to work for $\sigma < 20$ Mpc/h.

the real-space correlation function $\xi(r)$. We also use the simulations to test the validity of the 2-point correlation function model.

3.1 Errors in the redshift space correlation $\xi(\sigma, \pi)$

We calculate the 2-point correlation function in redshift space $\xi(\sigma, \pi)$ for each group mock, using a bin of 1Mpc/h. We can obtain a JK error for each mock, so a mean and dispersion for all the mocks. We compare it to the MC error, and to the analytical form, which is described in detail in paper I. We propose the error to have the following form $\Delta\xi = \Delta\xi_{\text{shot-noise}} + \Delta\xi_{\text{signal}}$, with two arbitrary coefficients α_{noise} and α_{signal} , so that:

$$\Delta\xi = \alpha_{\text{noise}} \Delta\xi_{\text{Poisson}} + \alpha_{\text{signal}} \xi \quad (11)$$

The comparison for the three kind of errors can be seen in Fig.1, where it is also plotted the JK error for real LRG galaxies, and the corresponding analytical error. The amplitude and shape of the error is similar in the group mocks and in LRG data, so we assume that our conclusions derived from the simulations can be translated to real LRG data. In order to see the differences in the mock errors with more detail, we fix the perpendicular distance σ for different cases and move along the line-of-sight π in Fig.2. The JK error starts to deviate slightly from MC for σ higher than 20Mpc/h, where the shot noise analytical form works perfectly. For small σ and π , the signal part of the analytical error helps to fit to MC error, but it seems that at these scales the best option is to use JK error. The covariance is lower than 0.2 for all the points, so it is nearly diagonal. In Fig.3 we compare the JK error and analytical error for real data for a bin of 0.2Mpc/h and we find similar conclusions. We have done the same analysis with dark matter simulations and they also work well, as expected. Note that contrary to what we found in paper I for 5Mpc/h binning, for smaller bins the shot noise model matches the expectations with $\alpha_{\text{noise}} = 1$, rather than $\alpha_{\text{noise}} = 1.4$. We believe that this could be related to the smaller covariance in 0.2Mpc/h and 1Mpc/h binning.

3.2 Errors in the projected correlation $\Xi(\sigma)$

We calculate the projected correlation function $\Xi(\sigma)$ for each group mock integrating through π the redshift space correlation function $\xi(\sigma, \pi)$, and we also calculate the JK error. Then we look at the difference between the MC dispersion and the mean over all the JK errors. In Fig.4, top panel, we see the mean $\Xi(\sigma)$ over all the simulations (solid line with errors), and over-plotted in blue big dots the $\Xi(\sigma)$ for the real LRG data. In the bottom panel we show a comparison of the different errors in the simulations (MC dotted line, and JK solid line with errors) and the error JK in the LRG data (big dots). Errors in MC and JK in simulations coincide at the scales where we can use the $\Xi(\sigma)$ (below 30Mpc/h). The JK error in LRG is also similar to the errors in the simulations. We have done the same analysis with dark matter simulations and they also work well, as expected. We conclude that using JK errors gives a good approximation to the true MC errors.

3.3 Errors in the real-space correlation $\xi(r)$

We now calculate the real-space correlation function $\xi(r)$ from the projected correlation function $\Xi(\sigma)$ (Eq.(9)). In Fig.5, top panel, we see the correlation function obtained from deprojecting $\Xi(\sigma)$ with errors (solid line) compared to the real-space correlation function which we can calculate

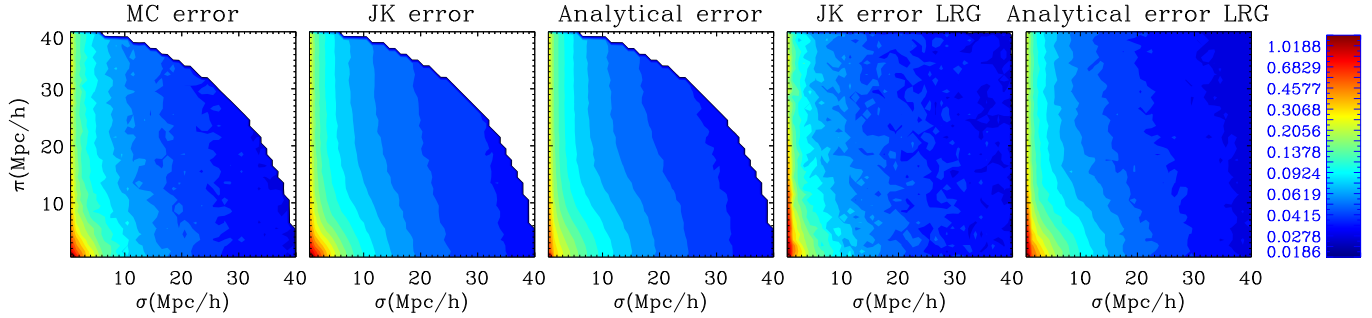


Figure 1. We compare different error estimators for $\xi(\sigma, \pi)$ with binning 1Mpc/h for MICE group mocks with $b = 1.9$: Monte Carlo, mean of all jackknife and analytical form. The last two plots refer to real LRG data: JK error and analytical form. Errors work well in the simulations, and they are similar in amplitude and shape to LRG real errors.

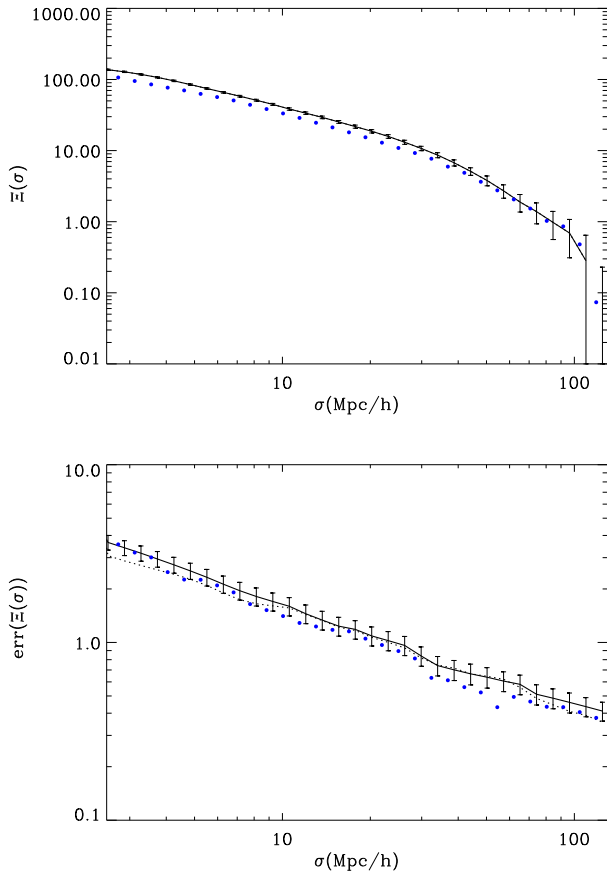


Figure 4. Top: $\Xi(\sigma)$ for the group simulations calculated from $\xi(\sigma, \pi)$ (solid line with errors) and the value for LRG data (big dots). Bottom: Errors in $\Xi(\sigma)$ for MC simulations (dotted line), JK simulations (solid line with errors) and JK for real LRG data (big dots)

using the simulations in real space, without redshift distortions (dotted line). We can see in Fig.5 how we recover well $\xi(r)$ for small scales (below 40Mpc/h). Over-plotted in blue (big dots), we see the real-space correlation function

obtained in LRG data, with a similar bias than the group simulations, as expected (b was found to be $b \simeq 2$ in Paper I). On the bottom panel of Fig.5, the plot compares errors in MC (solid line with errors) and JK (dotted line) case, and they are very similar at small scales. We have over-plotted the error JK in LRG data (big dots). We have also done a similar analysis with dark matter mocks and they also show a good agreement between JK and MC errors. As in the previous case, we conclude that using JK errors give a good approximation to the true MC errors.

3.4 Validity of the models

Besides studying errors, we also use the simulations to test the methods that we will apply to real data (LRG). In top panel of Fig.5 we showed that we can recover the real-space correlation function. Now we want to see if we can model the redshift-space correlation function with the simple model explained in §2, when taking the approximation of σ_{12} constant along the LOS and varying it for σ lower than 5Mpc/h. In Fig.6 we plot $\xi(\sigma, \pi)$ at small scales for the mean of the MICE dark matter mocks. We over-plot in solid lines our model with a varying pairwise velocity dispersion. We based this model on the pairwise velocity dispersion $\sigma_{12}(r)$ estimated from the velocities in the simulations. Fig.7 shows the measured pairwise velocity dispersion $\sigma_{12}(r)$. In our model, for σ larger than 5Mpc/h we use the effective $\sigma_{12} = 400\text{km/s}$ (asymptotic value at large scales). For σ lower than 5Mpc/h we use a different σ_{12} as given by Fig.7. With this simple approximation, we reproduce very well the observed FOG as shown in Fig.6. We have done this study with dark matter mocks since we know the variation of σ_{12} exactly, while when we construct the group mocks, we loose the pairwise velocity at small scales due to the way we identify groups.

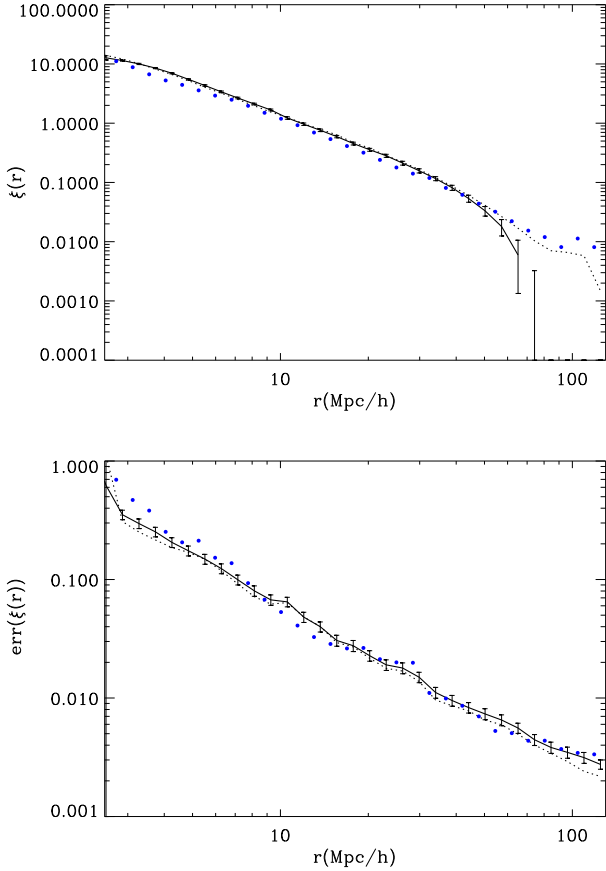


Figure 5. Top: $\xi(r)$ for the group simulations calculated from $\Xi(r)$ (solid line with errors) and the value for LRG data (big dots). Bottom: Errors in $\xi(r)$ for MC simulations (dotted line), JK simulations (solid line with errors) and JK for real LRG data (big dots)

4 THE DATA: LUMINOUS RED GALAXIES

SDSS luminous red galaxies (LRGs) are selected on the basis of color and magnitude to have a sample of luminous intrinsically red galaxies that extends fainter and farther than the SDSS main galaxy sample. Eisenstein et al (2001) give an accurate description of the sample. In Paper I we give more details of our selection. Here we just give a summary.

We k-correct the r magnitude using the Blanton program 'kcorrect'¹. We need to k-correct the magnitudes in order to obtain the absolute magnitudes and eliminate the brightest and dimmest galaxies. We have seen that the previous cuts limit the intrinsic luminosity to a range $-23.2 < M_r < -21.2$, and we only eliminate from the catalog some few galaxies that lay out of the limits. Once we have eliminated these extreme galaxies, we still do not have a volume limited for high redshift galaxies, but we suppose that the

¹ http://cosmo.nyu.edu/blanton/kcorrect/kcorrect_help.html

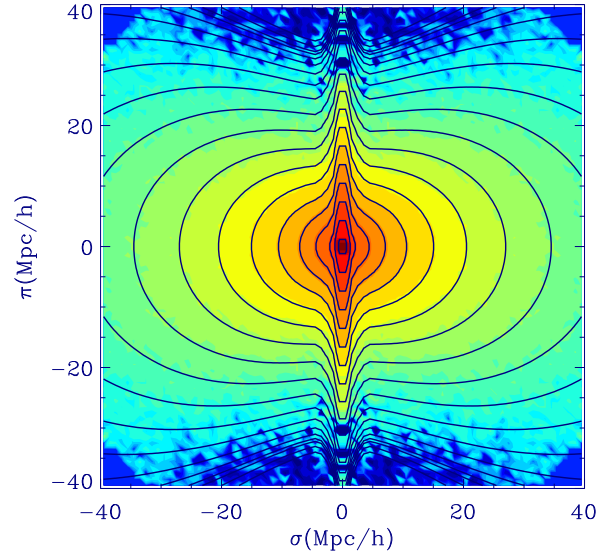


Figure 6. $\xi(\sigma, \pi)$ for the MICE dark matter simulation (as colors). The contour colors are -0.05, -0.01, -0.005, -0.001, 0, and 0.001 to 20 with 20 equally spaced logarithmic bins. In solid lines we have plotted the model for the input parameters of the simulation. For σ larger than 5Mpc/h we use the effective $\sigma_{12} = 400\text{km/s}$ (asymptotic value at large scales) to model $\xi(\sigma, \pi)$ while for σ lower than 5Mpc/h we use a different σ_{12} as seen in Fig.7, for each σ constant along the LOS π

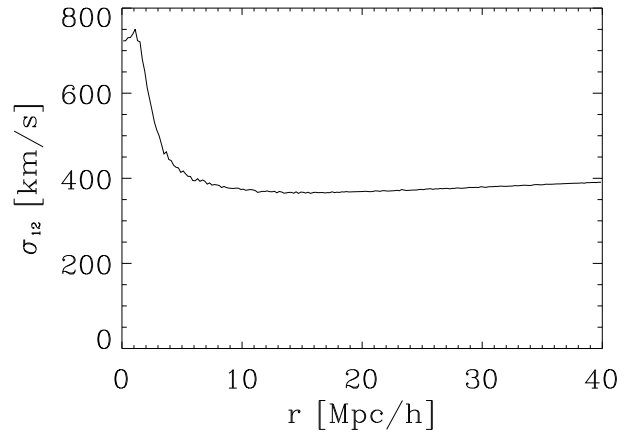


Figure 7. Dispersion in the pairwise velocity distribution σ_{12} estimated from the velocity field in the MICE dark matter simulations as a function of the distance between particles.

variations in luminosity just change the overall shape in the clustering.

We have masked the catalog using at the first step the photometric DR6 mask, based on the number of galaxies per pixel. In previous works we saw that the mask that we obtain statistically by dropping out the pixels with small number of galaxies gives the same correlation function that the one obtained by extracting the polygons masked by the

SDSS team. After that, we compare our masked catalog to the LRG spectroscopic catalog, and we extract the galaxies that lay outside from “good” plates.

This rough mask could imprint spurious effects at very small scales, but we are not interested in these scales where fiber collisions in the redshift catalog are limiting our analysis, for distances less than 55arc sec, less than 0.3Mpc/h at the mean redshift of LRG data, $z=0.35$. We obtain 75,000 galaxies for the final catalog, from $z=0.15$ to $z=0.47$. The area of the data used is around 13.5% of the sky. See Fig.2 in Cabré and Gaztañaga (2008) for a plot of the mask. Recently we have used another mask, provided by Swanson et al. (2008), which is in a readily usable form, translating the original mask files extracted from the NYU Value-Added Galaxy Catalog (Blanton et al. 2005), from MANGLE into Healpix format (Gorski et al. 1999), and results are very similar. We have also done the analysis with the recent data release DR7, the final one in SDSS, and results are very similar at small scales.

We use the ξ estimator of Landy and Szalay (1993),

$$\xi(\sigma, \pi) = \frac{DD - 2DR + RR}{RR} \quad (12)$$

to estimate the 2-point correlation function in redshift space, with a random catalog 20 times denser than the SDSS catalog. The random catalog has the same redshift distribution as the data, but smoothed to avoid the elimination of intrinsic correlations in the data, and also the same mask. We count the pairs in bins of separation along the line-of-sight (LOS), π , and across the sky, σ . The LOS distance is just the difference between the comoving distances in the pair. The perpendicular distance is $\sigma = \sqrt{s^2 - \pi^2}$, which corresponds approximately to the mean redshift.

5 ANALYSIS

As we explore small scales, we will show in this section that we encounter the following problems. First of all, the bias becomes clearly dependent on the scale for distances smaller than about 10 Mpc/h, because LRG are galaxies highly biased so they only keep the linear bias constant at large scales. Secondly, the model that we are using assumes that the pairwise velocity dispersion is independent of scale, which is not a good approximation for small scales as we have seen in the simulations. We can arrange this by using different σ_{12} for each real distance r , as explained in Section 2. Here we want to check if we can infer the correct variation of $\sigma_{12}(r)$ with scale using the $\xi(\sigma, \pi)$ data. As a test, we will compare the inferred values of $\sigma_{12}(r)$ with the direct measurement from the velocity field in the simulation.

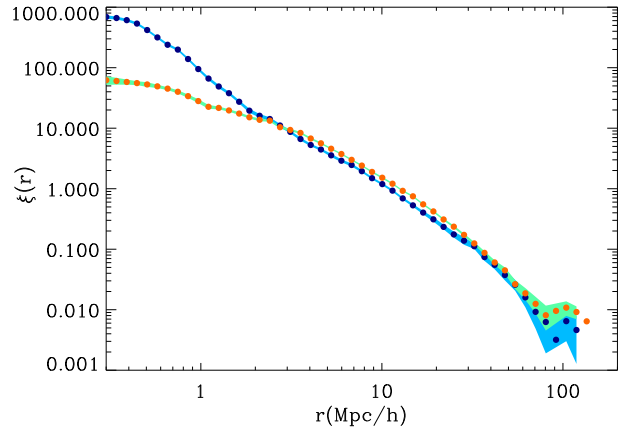


Figure 8. $\xi(r)$ (blue dots) and $\xi(s)$ (orange dots). We see clearly how the redshift-space correlation function is the real-space correlation function biased by a constant factor that represents gravitational infall (dependent on β in Kaiser approximation) at large scales above 4Mpc/h (although $\xi(r)$ is overestimated for scales larger than 30Mpc/h due to the precision in the calculation). However, for small scales, the redshift-space $\xi(s)$ is strongly suppressed compared to $\xi(r)$ due to random peculiar velocities.

5.1 Real space correlation

In Fig.8 we show the resulting real-space correlation function which we have calculated using Eq.(9) (in blue) and overplotted the monopole in redshift space (in orange). At intermediate scales, from 5 to 30 Mpc/h (the top value limited by the method to obtain $\xi(r)$), $\xi(s)$ is equal to $\xi(r)$ but biased by a constant factor, as in Eq.(10), due to Kaiser effect. We had shown this constant bias at intermediate scales (around 10Mpc/h) in Fig.8 of paper I (Cabré and Gaztañaga 2008), where we plot the ratio of the correlation function in redshift space and real space $\xi(s)/\xi(r)$. At large scales, we can associate it to a function of β obtained in Paper I at large scales. The agreement is excellent, which provides a good consistency check for our results. The difference between the real and redshift space correlation function at small scales is primordial due to the random peculiar velocities.

5.2 Power law fit

We next fit our estimation of the real space correlation function to a power law, $\xi(r) = (r/r_0)^{-\gamma_0}$, from 1Mpc/h to 15Mpc/h. At scales smaller than 1Mpc/h the fit is not good, it is no longer a power law. In Fig.9 we show a fit for r_0 and γ_0 . In Fig.10 we show the measured real space correlation function, the best fit power law model (red) and the dark matter non-linear correlation function obtained from best parameters in Paper I which works well for a linear bias, ie on large scales. The large scale and small scale fittings models agree well at large scales, as can be seen in the plot, and the correlation function does not follow a power law for distances smaller than ~ 1 Mpc/h, where we can probably

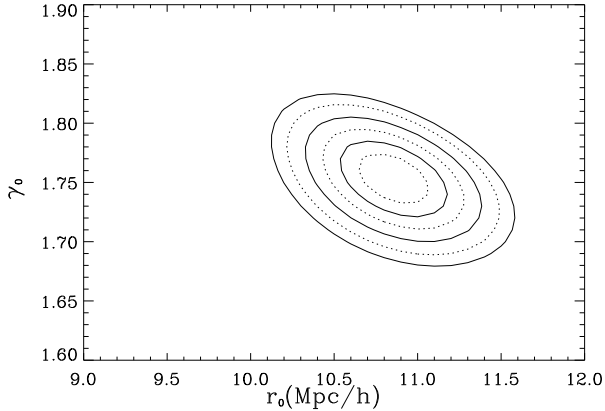


Figure 9. Best fit of γ_0 and r_0 of $\xi(r)$ to a power law model $\xi(r) = (r/r_0)^{-\gamma_0}$, 1-15Mpc/h. Dotted and continuous contours correspond to 1 ad 2 degrees of freedom with 1,2 and 3-sigma confidence.

see the transition from the one-halo to the two-halo term (Scoccimarro 2004).

These results are similar to other studies. Zehavi et al (2005) did a similar analysis with a previous SDSS spectroscopic data release (35000 LRGs) at intermediate scales from 0.3 to 40Mpc/h. We have doubled the number of LRGs and our results agree with them for the monopole, the projected correlation function, and the obtained real-space correlation function, with the same main conclusions. Also Eisenstein et al (2005), in a study of small scales (0.2-7Mpc/h) using the cross-correlation between spectroscopic LRG with the main photometric sample, remark that $\xi(r)$ can not be explained with a power-law fitting. However, Masjedi et al (2006) have obtained the correlation function at very small scales (0.01-8Mpc/h) and have found that, although with some features diverging from a power law, all the range is really close to a $\xi(r) \propto r^{-2}$.

5.3 Non-linear bias

We have checked in our simulations with halos that the non-linear bias typically follows a power-law (at least for distances larger than 0.3Mpc/h), which has a different slope γ_b depending on the halo mass. In general this could depend on other parameters concerning galaxy formation. LRG are assumed to be red galaxies that trace halos of $10^{13} M_\odot$, but there is a wide range of halo masses, and the non-linear bias shows us these properties. Here we estimate the bias as

$$b(r) = \sqrt{\xi(r)/\xi(r)_{DM}} = b_{nl}(r) \quad (13)$$

where we have separated the bias $b(r)$ into a constant scale independent term, b , on large scales and a function of scale $b_{nl}(r)$ which goes to unity on large scales. When $b_{nl}(r)$ reaches unity, we assume that the bias is linear from there

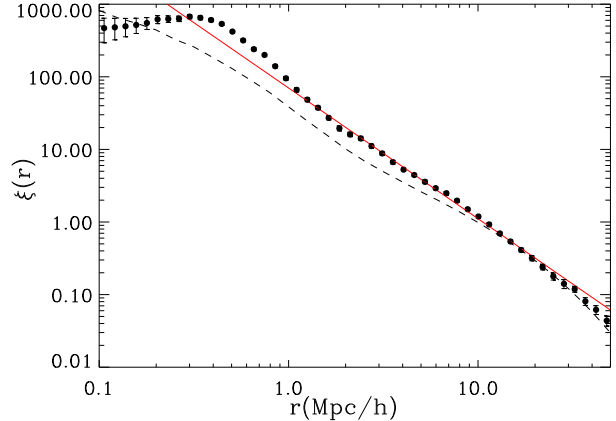


Figure 10. Observed $\xi(r)$ (symbols with errorbars), best fit to the power law $\xi(r) = (r/r_0)^{-\gamma_0}$ (red), and dashed over-plotted the best real space correlation function for large scales, assuming a constant bias

on. We define a parameter r_b for the power law $b_{nl}(r) = (r/r_b)^{-\gamma_b}$ which shows the scale from which non-linearity begins to be important. The value of r_b should coincide approximately with the correlation length, where the real space correlation function is unity.

To compute the non-linear bias $b(r)$ from the above equation, we need the dark matter correlation function and the linear bias b , which we have taken from the fitting at large scales done in Paper I. We have calculated the bias for all the values of Ω_m and different amplitudes. Then we marginalize over them. In Fig.11 we see the contours for r_b and γ_b (top panel), and the best fit (red in the bottom panel). This fit to the bias can explain the differences seen previously between the correlation function and a power law for scales smaller than 1Mpc/h. At scales smaller than 0.3Mpc/h, the real space correlation function turns down due to fiber collisions (Masjedi et al 2006). In detail, we see in Fig.11 a feature in the bias between 1 and 2 Mpc/h, indicating that LRGs galaxy bias is not completely smooth. We think that this feature is due to the range of halo sizes of our LRGs, which makes it difficult to predict exactly the transition point from the 1-halo to the 2-halo term (Scoccimarro 2004). If galaxies are residing within dark matter halos then the clustering of the galaxies on scales larger than halos is determined by the clustering of the dark matter halos that host them, plus statistics of the occupation of halos by galaxies. For larger scales than $\simeq 2$ Mpc/h (the biggest halos), the clustering comes entirely from LRGs that reside in different halos, while for smaller scales, the clustering can come from galaxies in different halos or galaxies in the same halo until it is reached a minimum size of halos (see Masjedi et al (2008) for a more detailed explanation).

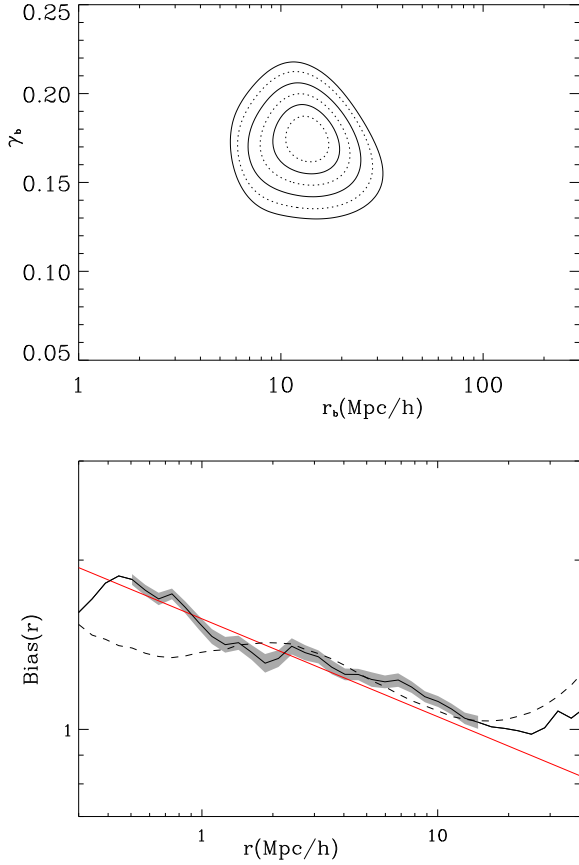


Figure 11. Top panel: Best fit to no linear bias $b_{nl}(r)$ (defined in the text) with a power law $b_{nl}(r) = (r/r_b)^{-\gamma_b}$. Bottom panel: Non linear bias $b_{nl}(r)$ (solid line with errors in gray) and best power law fit (red). We have also over-plotted in dashed line the bias obtained if we suppose that the galaxy correlation function is a power law.

5.4 Monopole and Quadrupole

Once we have obtained the real space correlation function, we can look at the monopole $\xi(s)$, the quadrupole $\xi_2(s)$ and also at $\xi(\sigma, \pi)$ in order to check the result. We see in Fig.12 the monopole $\xi(s)$ (top panel) and quadrupole $\xi_2(s)$ (bottom panel) binning the distance with 0.2Mpc/h, and over-plotted in red solid line the theoretical model, which we have found integrating $\xi(\sigma, \pi)$ and assuming a constant σ_{12} (derived using the normalized quadrupole $Q(s)$ in Paper I). The prediction uses the model explained above and in Paper I, where the shape of $\xi(\sigma, \pi)$ is given by the real-space correlation function and the parameters describing the velocity distortions. The monopole directly measured in the data (dots with shaded region in top panel of Fig.12) does not agree with the model (red line), which is lower for scales smaller than 3Mpc/h. The same happens to the quadrupole (bottom panel), where the model is also higher than the

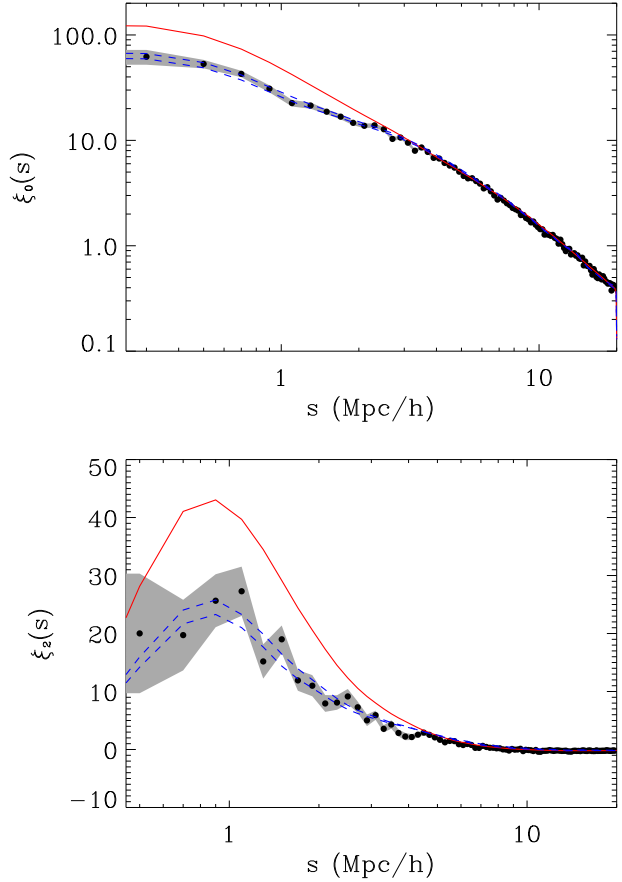


Figure 12. Monopole $\xi(s)$ (dots) with errors (gray), best model assuming a constant σ_{12} (solid red) and model assuming variation in σ_{12} with errors (dashed blue), as in Fig.15. Bottom panel: Quadrupole $\xi_2(s)$ (dots) as in the top panel.

measurements. These differences indicate that σ_{12} is higher at smaller scales as shown in Fig.7 for simulations.

5.5 Recovering σ_{12} from simulations

We now recover the dispersion of pairwise velocities σ_{12} at each perpendicular distance σ assuming that σ_{12} remains constant along the LOS π . In reality, σ_{12} is a function of the real distance r , $\sigma_{12}(r)$. At each π, σ , the correlation is a convolution of all the real distances. We could in principle try to fit all the π - σ plane for different shapes of $\sigma_{12}(r)$, but this involves too much freedom and such a fit is not feasible in practice. The alternatives are to do the fit in Fourier space, where there is no dependence of $\sigma_{12}(k)$ along the LOS, or to use the approximation $\sigma_{12}(r) \sim \sigma_{12}(\sigma)$ in the zone of the π - σ plane where this is a good approximation. We have studied the differences between $\xi(\sigma, \pi)$ obtained from either $\sigma_{12}(r)$ or from $\sigma_{12}(\sigma)$ to explore this later possibility. The two models differ, more or less strongly depending on the case, at small σ and large π . For our dark matter sim-

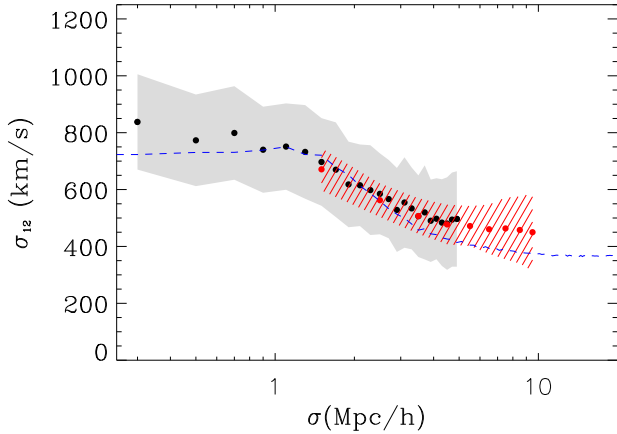


Figure 13. We plot the mean recovered $\sigma_{12}(r)$ ($\pi_{max} = 5Mpc/h$) for a bin $0.2Mpc/h$ (black circles with gray zone as errors) and for $1Mpc/h$ (red circles with dashed zone errors), compared to the original $\sigma_{12}(r)$ (dashed line) calculated in the real space simulation. We take each mock redshift space $\xi(\sigma, \pi)$ and model it following Eq.(3), from where we obtain the dependence of σ_{12} on the distance.

ulations, the differences are smaller than in the LRG case, where they can be large enough to bias the final result. The best option, then, is to fit for each perpendicular distance $\sigma_{12}(\sigma)$ using $\xi(\sigma, \pi)$ up to a maximum $\pi_{max} = 5 - 10Mpc/h$, where both models agree well. If we go further in π , the result is biased to lower values of σ_{12} .

In order to test the method to recover $\sigma_{12}(r)$ we have used our dark matter mocks, where we trust velocities to be accurate. We take each mock and recover $\sigma_{12}(r)$ for $\pi_{max} = 5, 10, 18, 30Mpc/h$. We have used a bin of $0.2Mpc/h$ for $\sigma = 0.3 - 5Mpc/h$ and a bin of $1Mpc/h$ for $\sigma = 1 - 10Mpc/h$. In Fig.13 we plot the mean recovered $\sigma_{12}(\sigma)$ for $0.2Mpc/h$ (black circles with gray zone as errors) and for $1Mpc/h$ (red circles with dashed zone errors), compared to the original $\sigma_{12}(r)$ calculated directly from velocities in the simulation (dashed line). We use $\pi_{max} = 5Mpc/h$ for this plot, but we obtain very similar results when we go further in π . The main conclusion of this analysis is that we recover correctly the random dispersion of pairwise velocities, and secondly that the method to derive σ_{12} works at least until $\pi_{max} = 30Mpc/h$, for dark matter. This method is good to obtain the variation of σ_{12} at small scales. At larger scales (around $5Mpc/h$), σ_{12} reaches a constant, and we see that in our study the estimated σ_{12} is slightly biased to higher values. At these distances, variations on σ_{12} do not change much the model for $\xi(\sigma, \pi)$, so this is not a problem for comparison to data. We should take into account that we are using a simplified model which assumes that pairwise velocities are exponential. This is a good approximation for small scales, as we see from the simulations, but the real dispersion is in fact skewed and it is not perfectly exponential, so we can see slight variations from the real dispersion.

However, to recover an unbiased result for σ_{12} from $\xi(\sigma, \pi)$, the most important point is to take into account the infall velocities in the model (Scoccimarro 2004). Here we include infall velocities through the parameter β .

We next calculate the χ^2 for each mock in the central region of the plane $\pi - \sigma$ (defined by the contours of $\xi(\sigma, \pi) > 1.0, 0.57, 0.43, 0.24$) and we obtain a mean and dispersion of the reduced χ^2 (ie the χ^2 divided by the number of degrees of freedom). The distribution of reduced χ^2 values from the different mocks can be seen in Fig.14, the mean is equal 1 and this means that the model works perfectly well for our simulations of dark matter. But note how the dispersion in the distribution of χ^2 is quite broad, there is therefore room for some divergences away from 1.

5.6 Measurement of σ_{12} as a function of scale

Once we have showed that we can recover $\sigma_{12}(r)$ and that this simple model works for dark matter, let's do the same for the LRG galaxies. In order to calculate the model $\xi(\sigma, \pi)$ at each σ and π , we need to assume the distortion parameter β and the real space correlation function $\xi(r)$. We use $\beta = 0.34$, found in Paper I of this series. We also use the real space correlation function $\xi(r)$ from the integration of $\xi(\sigma, \pi)$ along the line-of-sight, see Eq.(8) and Fig.8. As mentioned above, the real space correlation $\xi(r)$ is not well recovered above $30Mpc/h$, where we will use instead the measured monopole corrected by the distortion bias factor, Eq.(10). At large scales, the real space and the redshift space correlation function are almost linearly biased, except from the BAO peak where there are some smaller non-linear effects again, but these do not have an effect in the modelization of $\xi(\sigma, \pi)$ at small scales, so this is a good approximation. We calculate $\sigma_{12}(\sigma)$ up to $\pi_{max} = 5, 10, 15, 20, 25Mpc/h$. For values above $\pi_{max} = 10Mpc/h$, we find that $\sigma_{12}(\sigma)$ starts to be biased low for small values of σ with respect to the true values of $\sigma_{12}(r)$. For higher values of σ , we can fit until a larger π_{max} , reducing the errors. We use the same binning as in the simulations and the resulting $\sigma_{12}(r)$ is plotted in Fig.15, where we compare it to the true value from velocities in simulations (solid line). Both results have approximately the same amplitude, that depends strongly on the cosmological parameters. If there is no velocity bias, then our universe must be similar to our simulations.

Now we can recalculate the monopole and quadrupole including the variation of σ_{12} with scale. We obtain a good fit to the results, as we can see in Fig.12 (as a blue dashed line) compared to the same prediction assuming a constant σ_{12} (solid red line).

As mentioned in §1, Slosar et al (2006) show that pairwise velocity distribution in real space is a complicated mixture of host-satellite, satellite-satellite and two-halo pairs. The peak value is reached at around $1Mpc/h$ and does not reflect the velocity dispersion of a typical halo hosting these

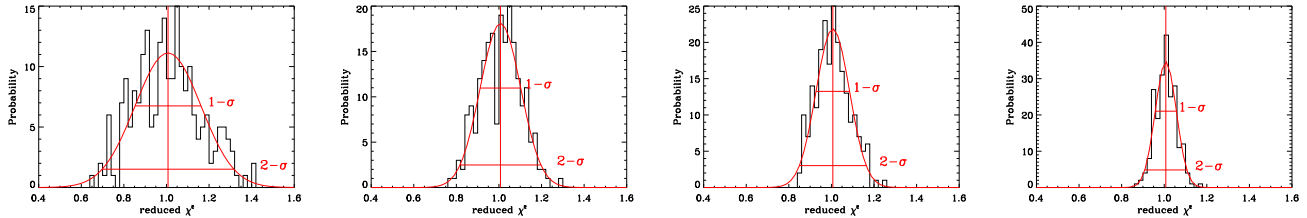


Figure 14. Distribution of χ^2 obtained from the mocks when we fit each $\xi(\sigma, \pi)$ with the dark matter model which includes the correct $\sigma_{12}(r)$. Different panels are showing the zone where we fit, from smaller to larger, for $\xi(\sigma, \pi) > 1., 0.57, 0.43, 0.24$

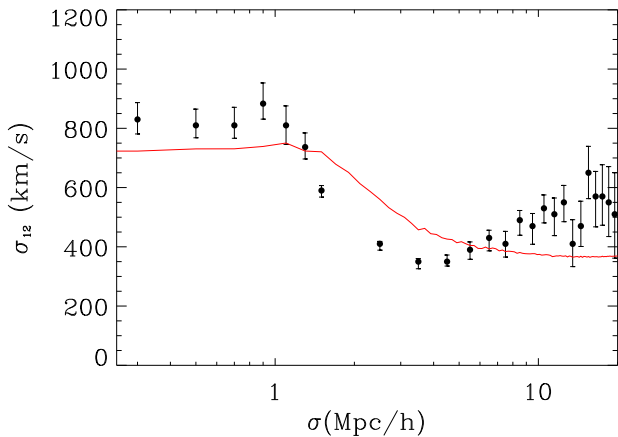


Figure 15. σ_{12} vs distance for LRG galaxies (circles with error-bars), obtained from modeling $\xi(\sigma, \pi)$ with Eq.(3). We compare it to the true value from velocities in the dark matter simulation (solid line).

galaxies, but is instead dominated by the sat-sat pairs in high-mass clusters. Tinker et al (2007) uses the HOD model to explain that at $r \sim 1 - 3$ Mpc/h, the PVD rapidly increases towards smaller scales as satellite-satellite pairs from massive halos dominate. At $r < 1$ Mpc/h, the pairwise velocities dispersion decreases with smaller separation because central-satellite pairs become more common, but we do not see this tendency because we do not study such small scales due to fiber collisions. At $r > 3$ Mpc/h, the σ_{12} is dominated by two-halo central galaxy pairs. Their predictions agree well with our results in shape and amplitude (compare Fig.15 with their Fig.4 more luminous prediction). Note that the amplitude of the predictions can be increased or reduced easily by changing the cosmological parameters.

Tinker et al (2007) also distinguish between $\sigma_{12}(r)$ and $\sigma_{12}(\sigma)$. They found that $\sigma_{12}(r)$ is larger than $\sigma_{12}(\sigma)$ (compare their Fig.4 with Fig.6). We have shown with our simulations that $\sigma_{12}(\sigma)$ can describe well $\sigma_{12}(r)$ provided π_{max} is small enough. Different groups have found this dependence of σ_{12} on the scale (Zehavi et al 2002, Hawkins et al 2003, Jing and Borner 2004, Li et al 2006, Van den Bosch 2007, Li et al 2007 and citations there). It is difficult to provide a detailed comparison with these previous results.

This is because very different assumptions are used: the infall model, the modeling of the real-space correlation, the values of π_{max} or the use of Fourier versus configuration space analysis. However, these previous results seem to find lower values of $\sigma_{12}(\sigma)$ than our results, obtaining a maximum pairwise velocities of around 600 km/s, rather than then 800 km/s that we find. We believe that this difference is mainly caused by the methodology, which can make $\sigma_{12}(\sigma)$ lower than $\sigma_{12}(r)$ when large values of π_{max} are used. In our case we find with our modeling that smaller values of π_{max} recover better the right values of $\sigma_{12}(r)$ when the galaxy bias b is large, as in the case of LRG. These larger values at $\sigma_{12}(r)$ agree well with the dark matter prediction for $\Omega_m = 0.25$ and $\sigma_8 = 0.85$, as found in paper I, so there is no need to postulate that LRG velocities are in any way different.

5.7 Consistency of $\sigma - \pi$ model: FOG

Now we look directly at $\xi(\sigma, \pi)$ at small scales once we have all the parameters, to see if the model works when we separate π and σ , for all the angles, rather than just the monopole or quadrupole. We have used a binning of 0.2Mpc/h for these plots, in order to see clearly the fingers of God, which are concentrated at very small σ . First, we can see the detailed plot of the measurements $\xi(\sigma, \pi)$ in Fig.16.

In the next three figures 17, 18 and 19, we show the differences between the data and the model in three cases. Top panels from left to right show: the data as colors; the data and the model over-plotted as solid line; and the model as colors. Bottom panels show: the same as in the top but we have zoomed the σ direction to see clearly the fingers of God.

In Fig.17, we compare the data with a model that assumes linear bias b (found fitting large scales only) and a constant pairwise velocity dispersion of σ_{12} (obtained from the quadrupole $Q(s)$). We see clearly that this does not work well. The FOG (along the π direction) are too small compare to data and the correlation in the σ direction has a different slope. This is partially due to the fact that the bias in the real data becomes non-linear on smaller scales. Part of the apparent lack of fingers of God in the models are corrected just adding the non-linear bias in the model.

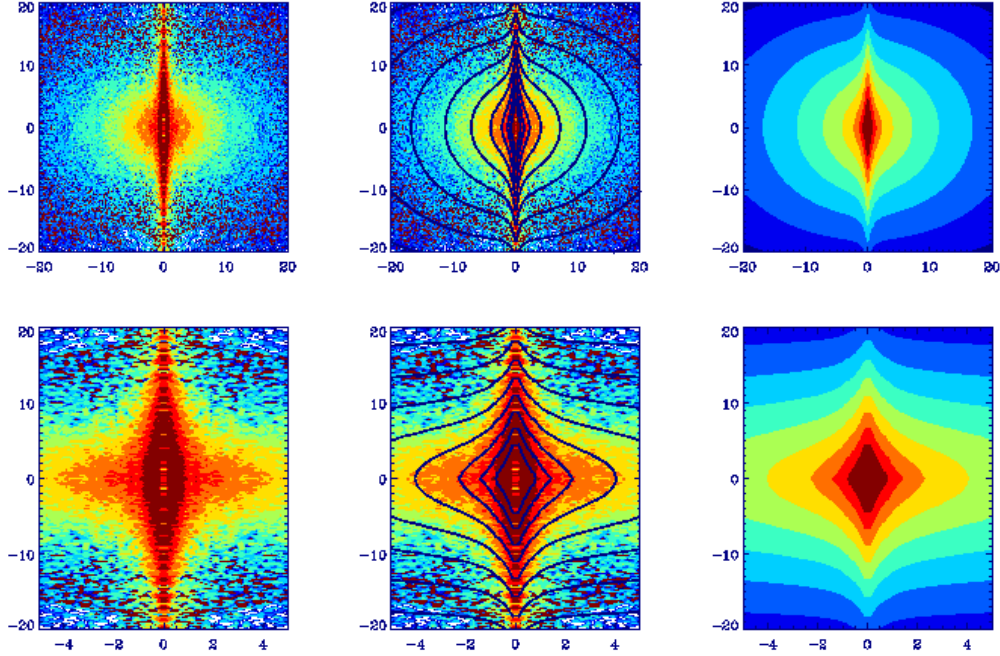


Figure 17. Redshift space 2-point correlation function $\xi(\sigma, \pi)$ (for the main slice in redshift $z=0.15-0.47$) modeled with a linear bias in the real-space correlation function, that we need to obtain $\xi(\sigma, \pi)$ with Eq.(3) and an effective $\sigma_{12}=380\text{km/s}$, as find for LRG at large scales. Top: data (as colors), data (as colors) + model (solid line), model (as colors). Bottom: the same zoomed in σ

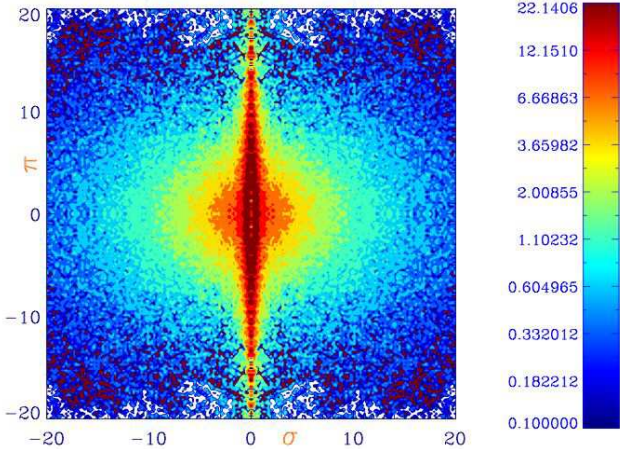


Figure 16. Redshift space 2-point correlation function $\xi(\sigma, \pi)$ calculated using squares in $\pi - \sigma$ of side= 0.2Mpc . Contours are: 0.1-50 with logarithm separation= 0.6 . We can see clearly the fingers of God in the line-of-sight direction

In Fig.18, we compare the model that we obtained using the real space correlation function just found, which includes all the non-linear effects, once we extrapolate $\xi(r)$ below 0.3Mpc/h , where fiber collisions prevent us from measuring clustering. We can see that we still need to explain the strong elongation we see in the direction line-of-sight,

which we correct with the third model in Fig.19. Here we include the variation of σ_{12} with scale, assuming that σ_{12} is constant for large scales and changes for small scales, as found in Fig.15. Here we use the exact modeling of $\sigma_{12}(r)$ as a function of r as explained in section 2. In order to see more clearly the validity of the model, we have plotted in Fig.20 the correlation function $\xi(\sigma, \pi)$ along the line-of-sight π for different fixed σ as indicated in the figure. Similar results are found for all other σ values, which is studied in bins of 0.2 Mpc/h . The model (smooth red solid line) seems to work well for small scales compared to the data (jagged lines with errors).

In the three cases, we can calculate the χ^2 to see how well the models fit to the data, as

$$\chi^2 = \sum_{\pi, \sigma} (\xi(\sigma, \pi)_{real} - \xi(\sigma, \pi)_{model})^2 / err(\pi, \sigma)^2 \quad (14)$$

using diagonal JK errors, which we have proved in the errors section that work for small σ . We have seen that the covariance is small (less than 20%) and so we believe that this χ^2 estimation should be accurate (at least to about 20% accuracy). We see how the χ^2 improves when we add a non-linear bias and variation of σ_{12} .

We calculate the χ^2 in different fitting zones, which we define by including in our analysis all the pixels that have an amplitude higher than 1.6, 2.4 or 4.4 in the third model,

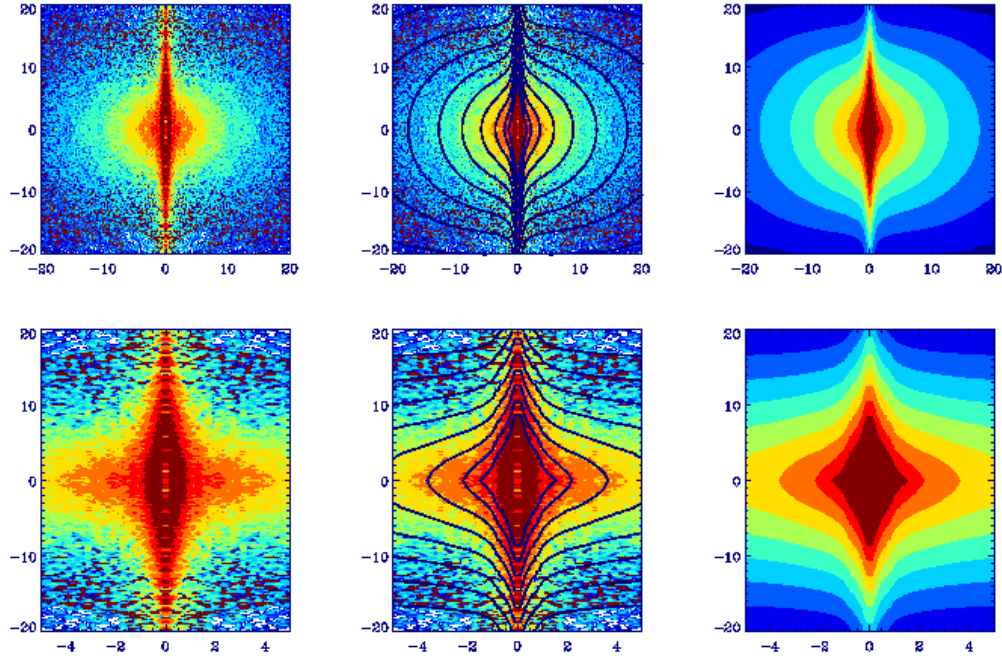


Figure 18. Redshift space 2-point correlation function $\xi(\sigma, \pi)$ ($z=0.15-0.47$) modeled with the real-space correlation function obtained from deprojection (this one has non-linear bias dependent on scale) and an effective $\sigma_{12}=380\text{km/s}$. We use Eq.(3) to calculate the model. Top: data (as colors), data (as colors) + model (solid line), model (as colors). Bottom: the same zoomed in σ

the one that is most similar to LRG (non-linear bias and variation of σ_{12}). The reduced χ^2 (total χ^2 divided by the number of individual points) varies from 2.2 to 3.2 for the first model (linear bias) depending on the fitting zone; from 1.8 to 2.8 for the second model (non-linear bias); and from 1.2 to 1.3 for the third model (non-linear bias and variation in σ_{12}). The third model represents a major improvement respect to the other models although the fit is not perfect because the reduced χ^2 is not equal to unity. However, the reduced χ^2 remains constant when changing the fitting zone, so the model is consistent at different scales. Moreover, at small scales, a reduced χ^2 of 1.2 is not rule out as can be seen in the first panel of Fig.14. Apart from this effect, we think that the difference to a perfect reduced χ^2 can be attributed to the covariance which is small but non zero for LRG and has been neglected in this analysis. We should also take into account that in order to recover σ_{12} we go through many steps, that can increase the error at the end. As an input for the calculation of the model of Eq.(3) we need β and the real-space correlation function $\xi(r)$, and both measures are estimations, they are not direct observables. We know that the model is perfect for dark matter, but it probably needs the inclusion of non-linearities to explain better the 2-halo pairwise velocity dispersions in highly biased galaxies as LRG (Scoccimarro 2004). We let to future work the inclusion of more realistic, non-linear corrections, to the Kaiser

model. As a conclusion, we see that this simple model can explain the strong FOG without need of having large pairwise velocities, and the model recovers almost all the features of $\xi(\sigma, \pi)$, a complicated mix of different effects, as explained in previous sections.

5.8 Different redshift slices

Finally, we look at the differences in the bias, defined in Eq.(13), for different redshift slices. In Paper I we saw that $b(z)D(z)$ was nearly constant as a function of redshift. This means that $b(z)$ grows smoothly with redshift in agreement to what we see in Fig.21. The slope in the non-linear bias is nearly the same, so the small scale interaction between galaxies is nearly the same as a function of redshift, as expected.

We have done the same analysis for different slices and the models for $\xi(\sigma, \pi)$ work very well for all the cases. Plots are very similar to the ones in previous section.

6 DISCUSSION

We have studied small scales in $\xi(\sigma, \pi)$ measured from luminous red galaxies, which have both a strong non-linear bias

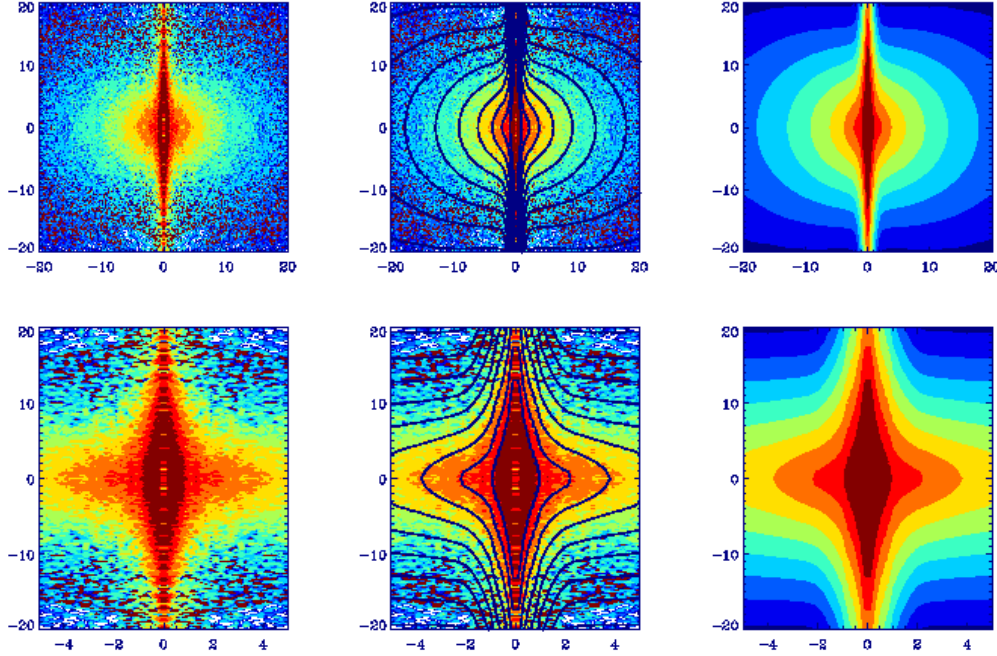


Figure 19. Redshift space 2-point correlation function $\xi(\sigma, \pi)$ ($z=0.15-0.47$) modeled with the real-space correlation function obtained from deprojection (using Eq.(3)) and σ_{12} dependent on scale, as plotted in Fig.15. We include the variation of σ_{12} with σ and assume that σ_{12} is constant along the line-of-sight for a fixed σ (perpendicular distance). Top: data (as colors), data (as colors) + model (solid line), model (as colors). Bottom: the same zoomed in σ

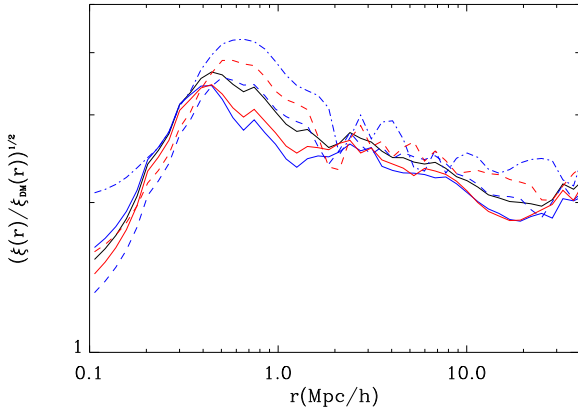


Figure 21. Comparison between the bias $b(r) = \sqrt{\xi(r)/\xi(r)_{DM}}$ (as in Eq.(13)) in real space for different slices in redshift. All: black, $z=0.15-0.3$ (solid blue), $z=0.3-0.4$ (dashed blue), $z=0.4-0.47$ (dashed-dotted blue); $z=0.15-0.34$ (solid red), $z=0.34-0.47$ (dashed red)

and are affected by large random peculiar velocities in redshift space. We have compared our results for the monopole in redshift space $\xi(s)$, the real-space correlation function $\xi(r)$ and the perpendicular projected correlation function $\Xi(r)$

with Zehavi et al (2005) and Masjedi et al (2006) results. Our analysis agree at all the scales except for very small scales, below 1Mpc/h, where we find some minor differences with respect to previous analysis.

Here we also recover, for the first time, the pairwise velocity dispersion σ_{12} of LRG galaxies as a function of separation by fitting $\xi(\sigma, \pi)$. Our method is shown to work in realistic simulations. We find that the scale variation of σ_{12} in LRG galaxies is similar to that in dark matter simulations. We show in section §5.7 that a simple Kaiser model convolved with an exponential distribution of pairwise velocities, can explain well the complicate shape of $\xi(\sigma, \pi)$ at small scales, once we add the scale dependent bias and the scale dependent σ_{12} . The χ^2 per degree of freedom reduces by over a factor of two when we allow b and σ_{12} to change with scale. We notice that if we attribute all the distortion at small scales to the peculiar velocities, without taking into account the non-linear bias, velocities appear to be artificially larger. On small scales the errors in $\xi(\sigma, \pi)$ are relatively small compare to the signal, see section §3.1. Thus the agreement of the $\xi(\sigma, \pi)$ data to our simple modeling shown in Fig.19 is quite remarkable and significant. We believe that this is the first time this simple $\xi(\sigma, \pi)$ model is shown to agree in detail with small scale LRG clustering.

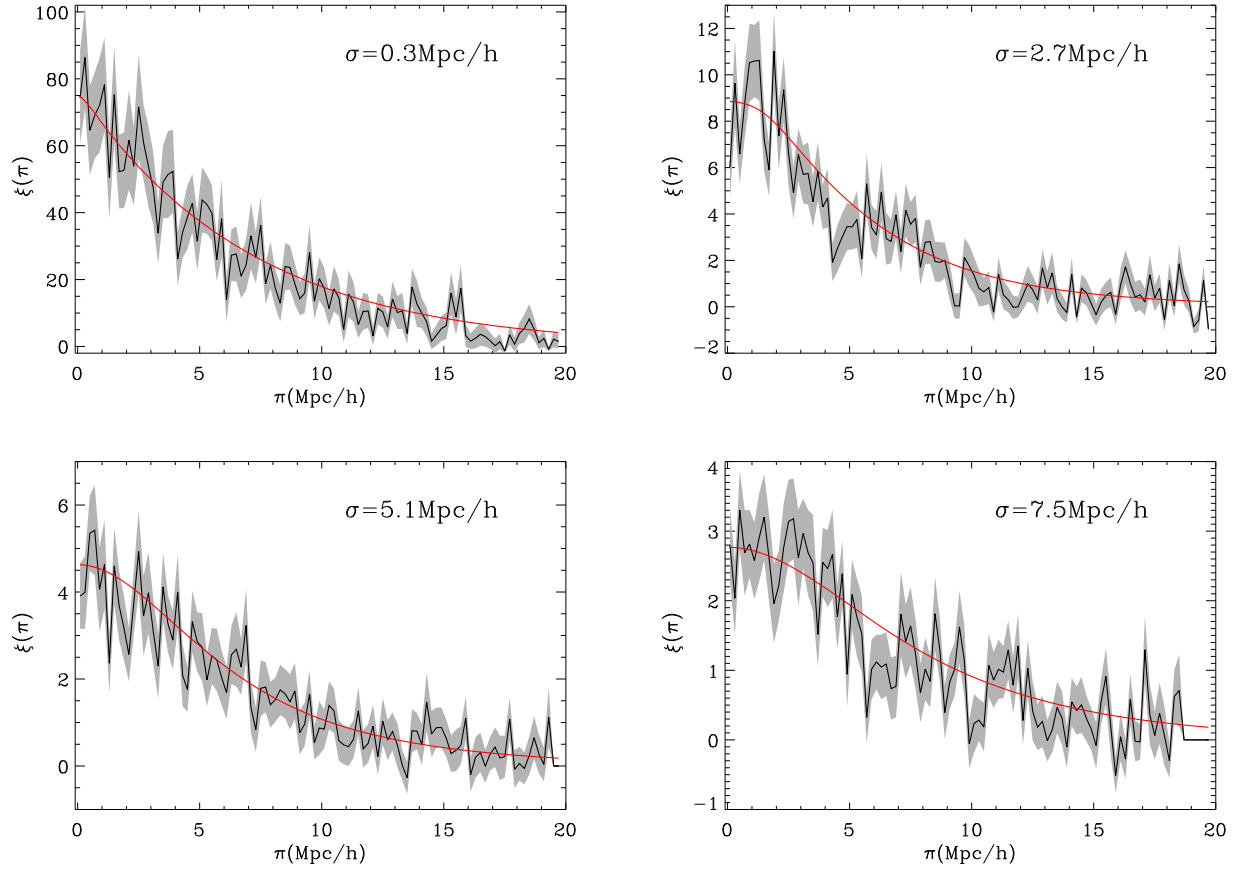


Figure 20. We plot $\xi(\sigma, \pi)$ as in Fig.19 along the line-of-sight π for different fixed σ in bins of 0.2 Mpc/h as labelled in the panels. Jagged solid line with errors (gray zone) is the measured LRG $\xi(\sigma, \pi)$ while the smooth line (red) is the best model (with non-linear bias and σ_{12} dependent on scale). Here we only show a few values of σ , but the model works well in all cases.

ACKNOWLEDGMENTS

We would like to thank Pablo Fosalba, Francisco Castander, Marc Manera and Martin Crocce for their help and support at different stages of this project. We acknowledge the use of simulations from the MICE consortium (www.ice.cat/mice) developed at the MareNostrum supercomputer (www.bsc.es) and with support from PIC (www.pic.es), the Spanish Ministerio de Ciencia y Tecnologia (MEC), project AYA2006-06341 with EC-FEDER funding, Consolider-Ingenio CSD2007-00060 and research project 2005SGR00728 from Generalitat de Catalunya. AC acknowledge support from the DURSI department of the Generalitat de Catalunya and the European Social Fund.

REFERENCES

- Adelman-McCarthy, J. K., et al., 2006, *ApJS*, 162, 38
Almeida C., Baugh C. M., Wake D. A., Lacey C. G., Benson A. J., Bower R. G., Pimbblet K., 2008, *MNRAS*, 386, 2145
Benson A. J., Baugh C. M., Cole S., Frenk C. S., Lacey C. G., 2000, *MNRAS*, 316, 107
Blanton M. R. et al., 2005, *AJ*, 129, 2562
Cabr e, A. and Gazta naga, E., astro-ph/0807.2460, *MNRAS* in press
Cannon, R. et al., 2007, *VizieR Online Data Catalog*, 837, 20425
da  ngela, J. , et al., 2008, *MNRAS*, 383, 565
Davis, M. and Peebles, P. J. E., 1983, *APJ*, 267, 465
Eisenstein, D. J. and Hu, W., 1998, *APJ*, 496, 605
Eisenstein et al., 2001, *AJ*, 122, 2267
Eisenstein D. J., Blanton M., Zehavi I., Bahcall N., Brinkmann J., Loveday J., Meiksin A., Schneider D., 2005, *APJ*, 619, 178
Gorski K. M., Wandelt B. D., Hansen F. K., Hivon E., Banday A. J., 1999, eprint arXiv:9905275
Hamilton, A. J. S., 1992, *APJL*, 385, L5
Hawkins, E. et al., 2003, *MNRAS*, 346, 78
Jackson, J., 1972, *MNRAS*, 156, 1P
Jing, Y. P. and B rner, G., 2004, *MNRAS*, 617, 782
Kaiser, N., 1987, *MNRAS*, 227, 1
Landy, S. D. and Szalay, A. S., 1993, *APJ*, 412, 64
Li C., Jing Y. P., Kauffmann G., B rner G., White S. D. M., Cheng F. Z., 2006, *MNRAS*, 368, 37
Li C., Jing Y. P., Kauffmann G., B rner G., Kang X., Wang L., 2007, *MNRAS*, 376, 984
Mandelbaum R., Seljak U., Cool R. J., Blanton M., Hirata C. M., Brinkmann J., 2006, *MNRAS*, 372, 758
Masjedi, M., et al., 2006, *APJ*, 644, 54

- Masjedi M., Hogg D. W. and Blanton M. R., 2008, APJ, 679, 260
Matsubara, T., 2000, APJ, 535, 1
Peebles, P. J. E. 1980, *The Large-Scale Structure of the Universe*
(Princeton, NJ: Princeton University Press)
Ross, N. P., et al., 2007, MNRAS, 381, 573
Saunders, W. and Rowan-Robinson, M. and Lawrence, A., 1992,
MNRAS, 258, 134
Soccimarro, R., 2004, PRD, 70, 8
Slosar A. and Seljak U. and Tasitsiomi A., 2006, MNRAS, 366,
1455
Smith, R. E., et al., 2003, MNRAS, 341, 1311
Swanson M.E.C., Tegmark M., Blanton M., Zehavi I., 2008, MN-
RAS, 385, 1635
Szalay, A. S. and Landy, S. D. and Broadhurst, T. J., 1998, Pro-
ceedings of the 12th Potsdam Cosmology Workshop, 111-112
Szapudi, I., 2004, APJ, 614, 51
Tinker J. L. and Norberg P. and Weinberg D. H. and Warren
M. S., 2007, APJ, 659, 877
van den Bosch F. C., Yang X., Mo H. J., Weinmann S. M, Macciò
A. V, More S., Cacciato M., Skibba R., Kang, X.
Wake, D. A., et al., 2008, MNRAS, 387, 1045
Zehavi, I., et al., 2002, APJ, 571, 172
Zehavi, I., et al., 2005, APJ, 621, 22